Nano Research 2014, 7(7): 1007–1017
DOI 10.1007/s12274-014-0464-5
Research Article

ISSN 1998-0124
CN 11-5974/O4

A nanoporous oxide interlayer makes a better Pt catalyst on a metallic substrate: Nanoflowers on a nanotube bed

Hongyi Li[1,2], Jinshu Wang[1] (✉), Man Liu[1], Hong Wang[1], Penglei Su[1], Junshu Wu[1], and Ju Li[2] (✉)

[1] *Key Laboratory of Advanced Materials, College of Materials and Engineering, Beijing University of Technology, Beijing 100124, China*
[2] *Department of Nuclear Science and Engineering and Department of Materials Science and Engineering, Massachusetts Institute of Technology, Cambridge, Massachusetts 02139, USA*

Received: 20 December 2013
Revised: 21 February 2014
Accepted: 31 March 2014

© Tsinghua University Press and Springer-Verlag Berlin Heidelberg 2014

KEYWORDS
electrocatalyst,
titanium dioxide nanotube,
platinum nanoflower,
catalytic activity,
cycle life

ABSTRACT

To improve the contact between platinum catalyst and titanium substrate, a layer of TiO_2 nanotube arrays has been synthesized before depositing Pt nanoflowers by pulse electrodeposition. Dramatic improvements in electrocatalytic activity (3×) and stability (60×) for methanol oxidation were found, suggesting promising applications in direct methanol fuel cells. The 3× and 60× improvements persist for Pt/Pd catalysts used to overcome the CO poisoning problem.

1 Introduction

Due to superior catalytic activity and chemical stability, nanostructured platinum (Pt) is frequently used in fuel cells [1–4], metal–air batteries [5–8], water ionizers [9, 10], solar cells [11–14], and bio-sensors and actuators [15–18]. The high price of Pt drives nanostructuring strategies to reduce platinum mass use, while maintaining total electrode activity and stability [19]. Platinum mass use can be reduced by optimizing platinum particle's morphology and size due to surface structure effects on catalytic activity [20, 21]. Therefore, bonding Pt nanoparticles with controlled morphology and size on a metal substrate, such as titanium (Ti), may dramatically reduce Pt mass use for electrocatalysis [3]. However, the poor contact between Pt nanoparticles and Ti substrate often leads to mechanical detachment, loss of electron conduction paths, and greatly reduced service life. Because a Pt nanoparticle has a small radius of curvature (r_{Pt}), it cannot bond well with an atomically flat surface ($r_{substrate} = \infty$) according to the Johnson–Kendall–Roberts (JKR) theory of adhesive contact. Roughening the substrate surface by nanostructuring, so that its radius of curvature matches

Address correspondence to Jinshu Wang, wangjsh@bjut.edu.cn; Ju Li, liju@mit.edu

that of the nanoparticle, may significantly improve bonding. Anodic oxidation dramatically increases the roughness and surface area of Ti [22–29], and thus could be a viable strategy to achieve the above goal. Lei et al. have previously deposited Pt nanospheres on a titanium substrate with TiO_2 nanotube arrays and found improved specific catalytic activity of Pt [30]. However, they used single-pulse electrodeposition, which gives a low Pt loading (0.1 mg/cm^2).

In the present work, Ti substrates were first anodized in an organic electrolyte containing fluoride ions [31]. TiO_2 nanotube arrays, with diameter of ~80 nm and length of ~2 μm, were formed on the surface of the Ti substrate. Pt nanoflowers were then deposited on the surface of anodized Ti containing TiO_2 nanotubes (Pt–TNT–Ti), and normal Ti with a compact thin oxide film of ~100 nm thickness (Pt–Flat–Ti), using pulse electrodeposition (PED). The hybrid electrodes' electrocatalytic activity and stability were investigated in sulfuric acid solution with or without methanol fuel. The measurements show that not only the electrocatalytic activity but also the chemical stability of the hybrid electrode was greatly increased by nanostructuring the Ti surface. Essentially, planting Pt nanoflowers on nanotube beds (Pt–TNT–Ti) was found to work much better than planting the same Pt nanoflowers on flat beds (Pt–Flat–Ti). It is also intriguing that the micron-long TiO_2 nanotubes do not seem to impede electron transfer between Pt and the titanium metal, and actually reduce the electrical impedance by a factor of two compared to Pt–Flat–Ti.

2 Results and discussion

Figure 1 briefly illustrates our approach. The Ti substrate was first nanostructured by anodic oxidation (Fig. 1(a)), followed by annealing to transform the anodized amorphous TiO_2 into anatase (Fig. 1(c)). For comparison, the pure titanium substrate was annealed in an oxygen atmosphere to form a compact oxide film of ~100 nm thickness on the Ti substrate (Fig. 1(b)). The Pt nanoflowers were deposited on the different substrates as shown in Fig. 1. In order to examine the efficacy of the "flower-on-stem" approach, the electrochemically active surface area, electrocatalytic capability for methanol oxidation and conductivity of the hybrid electrode in methanol plus sulfuric acid solution were measured and compared.

With anodization, a 2 μm-thick layer of an aligned amorphous TNT array with openings of 80 ± 5 nm was created on top of a more compact TiO_2 underlayer that touches the Ti metal (Fig. 1(a)). To obtain crystalline TiO_2, the amorphous TNT thin film was converted into the anatase phase by annealing at 500 ℃ for 2 h [31, 32]. Figures 2(a) and 2(b) show the top and cross-sectional morphologies of the annealed TNT thin film. The conversion from amorphous to anatase phase was identified by XRD (Fig. 1(c)). The platinum nanoparticles aggregate in the form of nanoflowers which mainly cover the top surface of the TiO_2 nanotube array (Pt–TNT–Ti), and also partly disperse along the wall of the nanotubes (Fig. 2(d)). Compared with the reported pulse method (–2 mA/cm^2) for electrodepositing Pt nanoflowers [30], we adopted higher pulse current (J_{pulse} = –350 mA/cm^2) for a relatively long duration (6 ms), which not only reduces the deposition time but also makes the Pt nanoflowers more homogenously distributed. In comparison to direct current deposition (0.1 mA/cm^2 reported by Zhang [33]), the high current densities increased the number of deposition centers (nucleation sites) around the tubes. The relaxation time (zero current density), t_{off}, improved the homogeneity of the deposition and limited hydrogen evolution [34, 35]. For comparison, Pt nanoflowers were also electrodeposited on the surface of titanium with native TiO_2 (Pt–Flat–Ti). It is clear that Pt nanoflowers can also be electrodeposited on the surface of the TiO_2 film and the particle size is similar to that of Pt–TNT–Ti. However, there are some cracks between the Pt nanoflower layer and TiO_2 thin film (Fig. 2(f)), indicating poor bonding as hinted before. XRD shows that the nanoflowered Pt had (111), (200) and (220) diffraction peaks, as shown in Fig. 1(c), characteristics of a face-centered cubic (FCC) crystal structure. It can also be seen that the diffraction peak intensities of the (111) and (200) peaks are higher than that of (220), which is in agreement with the TEM results (see below). The average particle size of the Pt particles was calculated to be about 7.2 nm for Pt–TNT–Ti and 7.3 nm for Pt–Flat–Ti based on the Scherrer equation. The TiO_2 nanotubes are in the anatase phase, as shown in the top XRD pattern in Fig. 1(c).

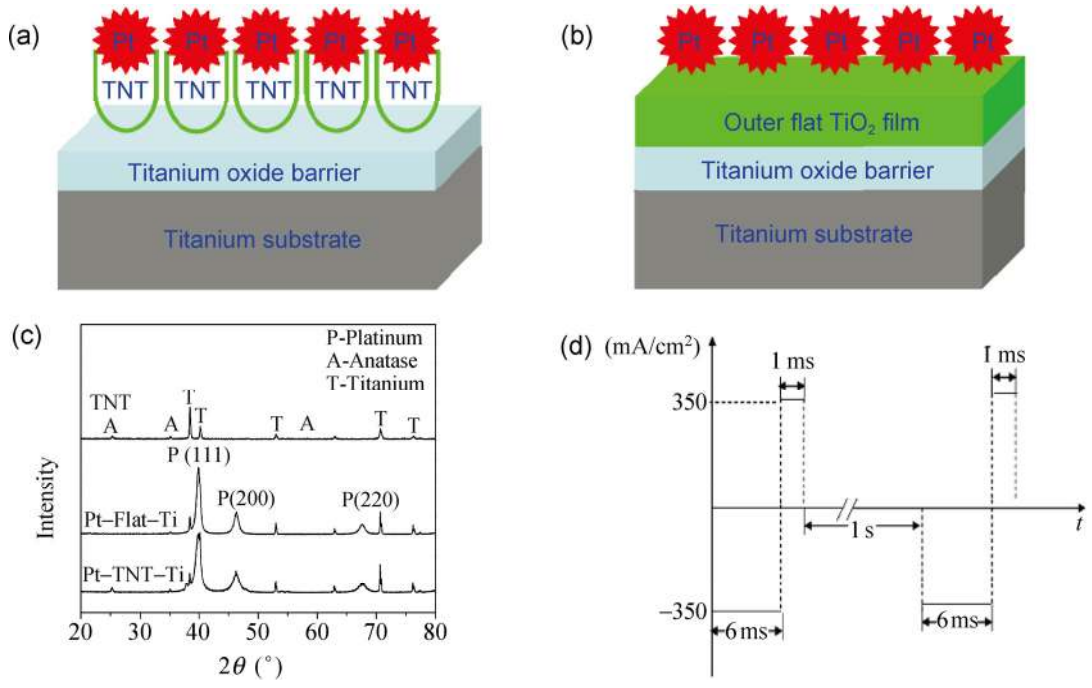

Figure 1 (a) Illustration of Pt nanoflowers on the TiO_2 nanotube array substrate and (b) the flat TiO_2 film substrate; (c) XRD patterns of Pt–TNT–Ti, Pt–Flat–Ti and annealed TiO_2 nanotube arrays and (d) the schematic of the current pulse shape utilized during the Pt electrodeposition process.

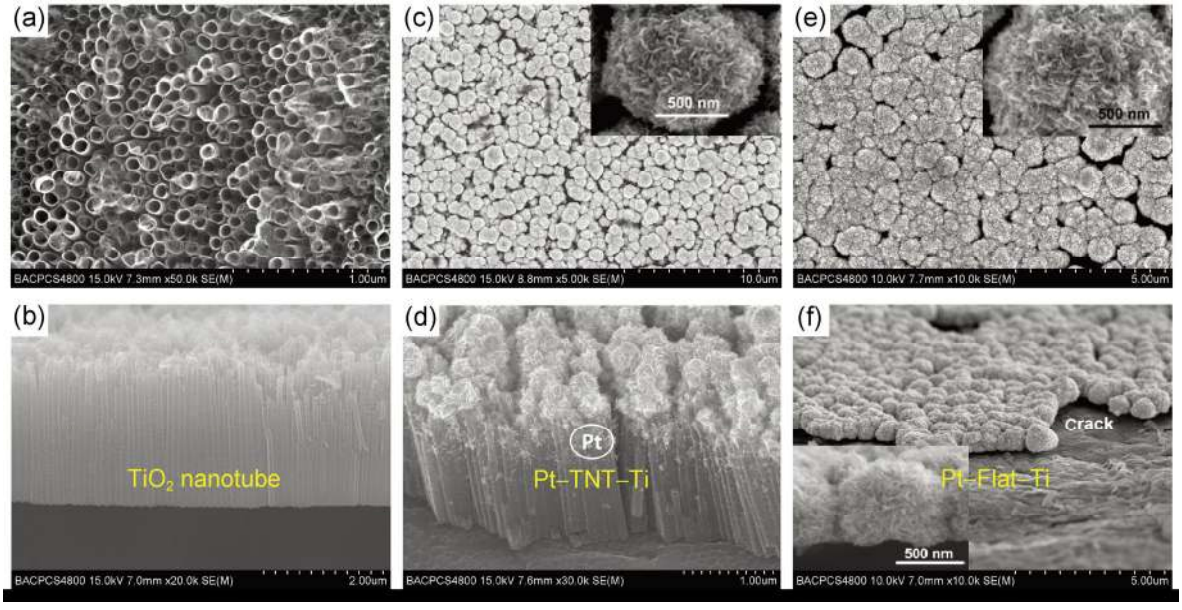

Figure 2 Scanning electron microscopy morphology of the TiO_2 nanotube (TNT) thin film and the hybrid electrode films decorated with Pt nanoflowers: (a) top view of TNT, (b) cross-section of TNT, (c) top view of Pt–TNT–Ti, (d) cross-section of Pt–TNT–Ti, (e) top view of Pt-Flat-Ti and (f) cross-section of Pt–Flat–Ti. The insets in (c) and (e) are high-magnification views of the top morphology of Pt–TNT–Ti and Pt–Flat–Ti respectively. The inset in (f) is the high-magnification cross-section of the Pt nanoflower layer of Pt–Flat–Ti.

The morphologies of the Pt nanoflowers are shown in Fig. 3. The diameters of the nanoflowers ranged from 0.6 μm to 0.8 μm, as calculated from Fig. 3(a). The surface of the nanoflower was composed of Pt nanoparticles, as identified by the HRTEM images (Fig. 3(d)). The particle size was calculated to be 7–9 nm, which is consistent with the size calculated from XRD patterns (Fig. 1(c)) based on the Scherrer

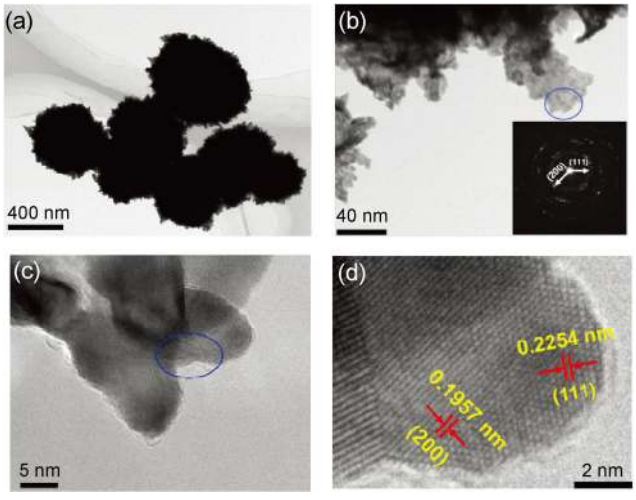

Figure 3 Transmission electron microscopy observation of nanoflowers with different magnification: (a) and (b) are low-magnification views of Pt nanoflowers; (c) and (d) are HRTEM images of the morphology of Pt nanoparticles that make up the Pt nanoflower.

equation. The HRTEM images also clearly show that main orientation was Pt (111) and Pt (100), in good agreement with the XRD results.

The mechanism for the formation of Pt along the wall of the nanotubes is that the bottom of the TNT has a lower potential than that of the top section. The lower potential resulted in the $Pt^{IV}Cl_6^{2-}$ ion being preferentially reduced to pure Pt along the wall. However, the $Pt^{IV}Cl_6^{2-}$ ions could not be immediately replaced because of the low concentration of $Pt^{IV}Cl_6^{2-}$ ions in the precursor. Therefore, the Pt was not uniformly deposited into the nanotubes as in the case of Ni in an anodic aluminium oxide (AAO) template [34] and Cu in TiO_2 nanotubes [35].

Figure 4 describes the cyclic voltammograms (CVs) of samples in 0.5 M H_2SO_4 (with no methanol fuel) at a potential scan rate of 50 mV/s. Similar responses were noticed in the potential between –0.25 V and 0.0 V for Pt–TNT–Ti and Pt–Flat–Ti. Three well-defined hydrogen adsorption peaks at about –0.24 V, –0.15 V and 0.0 V are observed for Pt–TNT–Ti, which are respectively attributed to the surface adsorption characteristics of Pt (111), Pt (100) and Pt (110) facets, indicating that these Pt nanoflowers have good

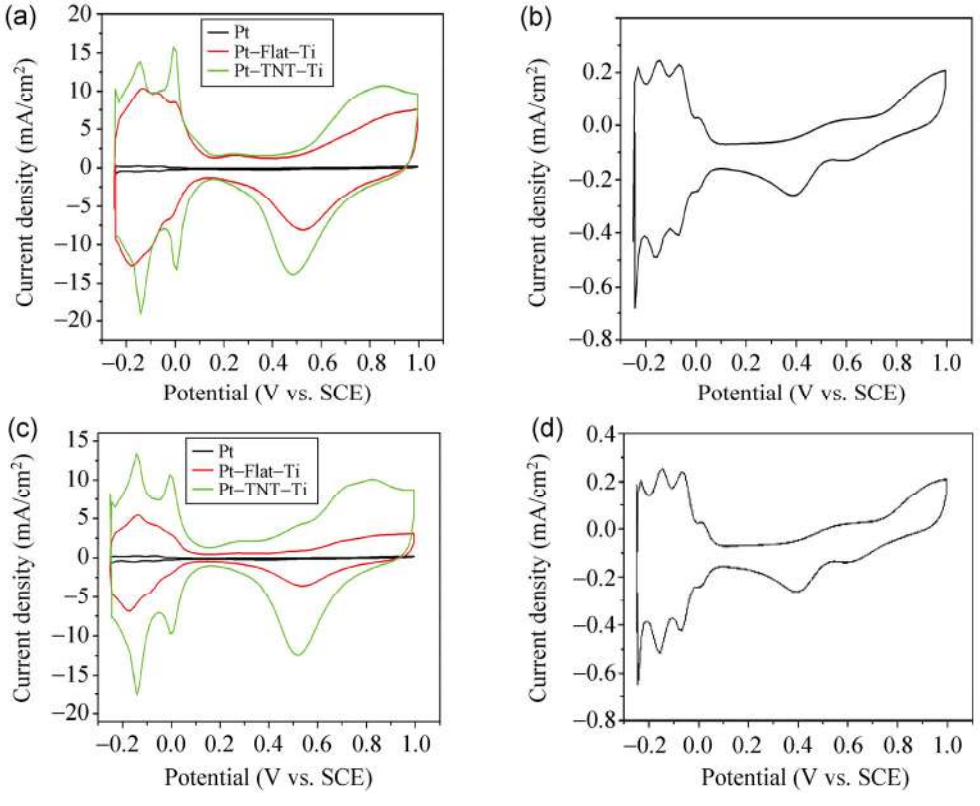

Figure 4 CVs of Pt–TNT–Ti (green), Pt-Flat-Ti (red) and pure platinum plate (black) in 0.5 M H_2SO_4 solution with a scanning rate of 50 mV/s: (a) and (b) were tested using the as-deposited electrode; (c) and (d) were tested after the chronoamperometric experiment; (b) and (d) are the curves for the pure platinum electrode with an expanded current density scale.

crystalline facets, in agreement with the XRD and HRTEM results.

Hydrogen adsorption and desorption is a powerful technique to determine the active surface area of a Pt electrode, and the integrated intensity of the peaks represents the number of Pt sites available for hydrogen adsorption/desorption, that is, the true surface area. By means of hydrogen adsorption/desorption methods and CV, the electrochemical surface area of Pt nanoflower thin films can be calculated as [19]:

$$s_{EI} = \frac{Q_H}{Q_{ref} \times Pt_{loading}} \quad (1)$$

where Q_H(mC/cm^2) is the number of catalytic sites available for hydrogen adsorption/desorption, and Q_{ref} = 0.21 mC/cm^2, is the charge needed for oxidation of a single layer of hydrogen on a smooth Pt surface. The Q_H values of Pt nanoflower thin films measured under the electro-adsorption curve for hydrogen were 58.37 mC/cm^2 and 42.75 mC/cm^2 for Pt–TNT–Ti and Pt–Flat–Ti, respectively. The active surface areas of Pt were calculated to be 228.3 cm^2/mg and 225.5 cm^2/mg for Pt–TNT–Ti and Pt–Flat–Ti, respectively.

The electrocatalytic activity of the samples was evaluated using cyclic voltammograms (CV) in 1.0 M methanol fuel plus 0.5 M sulfuric acid electrolyte. The results are summarized in Table S1 (in the Electronic Supplementary Material (ESM)). Figure 5(a) illustrates the CV curves for Pt–TNT–Ti and Pt–Flat–Ti at 50 mV/s. The forward anodic current density peak (F_p) of methanol electro-oxidation reached up to 149.6 mA/cm^2 for Pt–TNT–Ti and 96.0 mA/cm^2 for Pt–Flat–Ti (previously reported results were ~21 mA/cm^2 for a Pt/nanotube (NT) electrode [36]). All the current densities reported here were normalized to the electrode geometry area, i.e., the nominal area of the electrode. The current density of Pt–TNT–Ti is even higher than that of Pt–Flat–Ti, which is the main reason why the F_p peak current position (0.741 V) of Pt–TNT–Ti is slightly higher than that (0.717 V) of Pt–Flat–Ti, due to the resistance polarization. A possible reason for the observed superiority is that the conductivity of Pt–Flat–Ti is lower than that of Pt–TNT–Ti because the contact area between Pt and

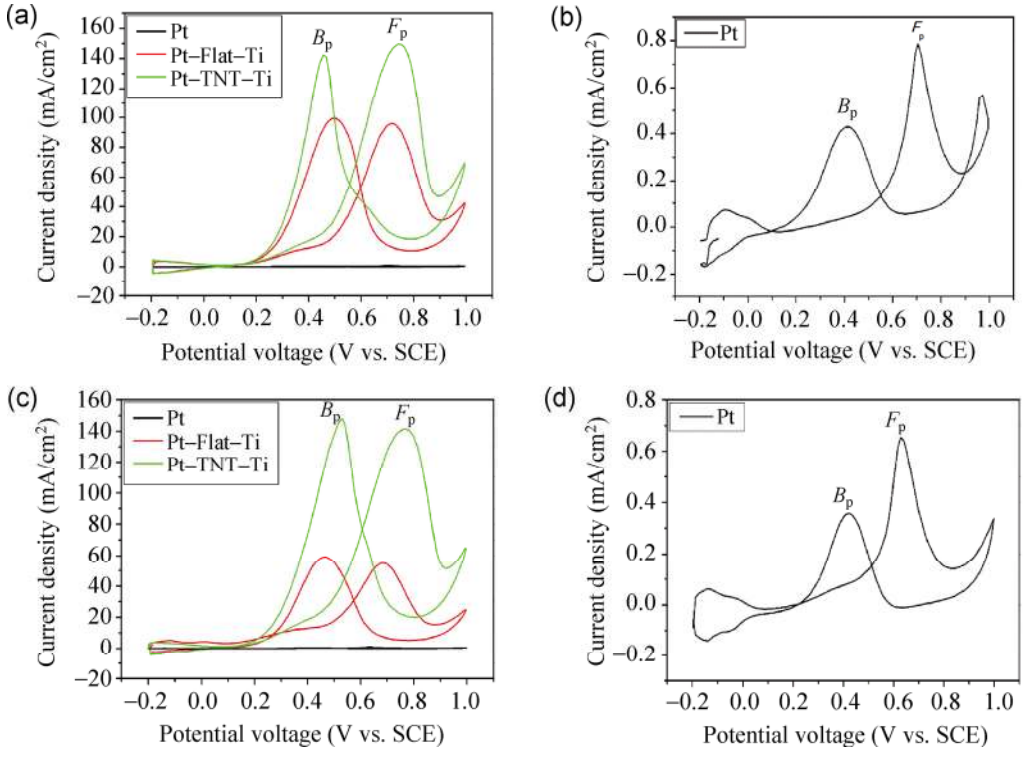

Figure 5 CVs of Pt–TNT–Ti (green), Pt–Flat–Ti (red) and pure platinum plate (black) in 1.0 M methanol fuel plus 0.5 M H_2SO_4 solution with a scanning rate of 50 mV/s: (a) and (b) were tested with the as-deposited electrode; (c) and (d) were tested after the chronoamperometric experiment; (b) and (d) are the curves for pure platinum electrode with an expanded current density scale.

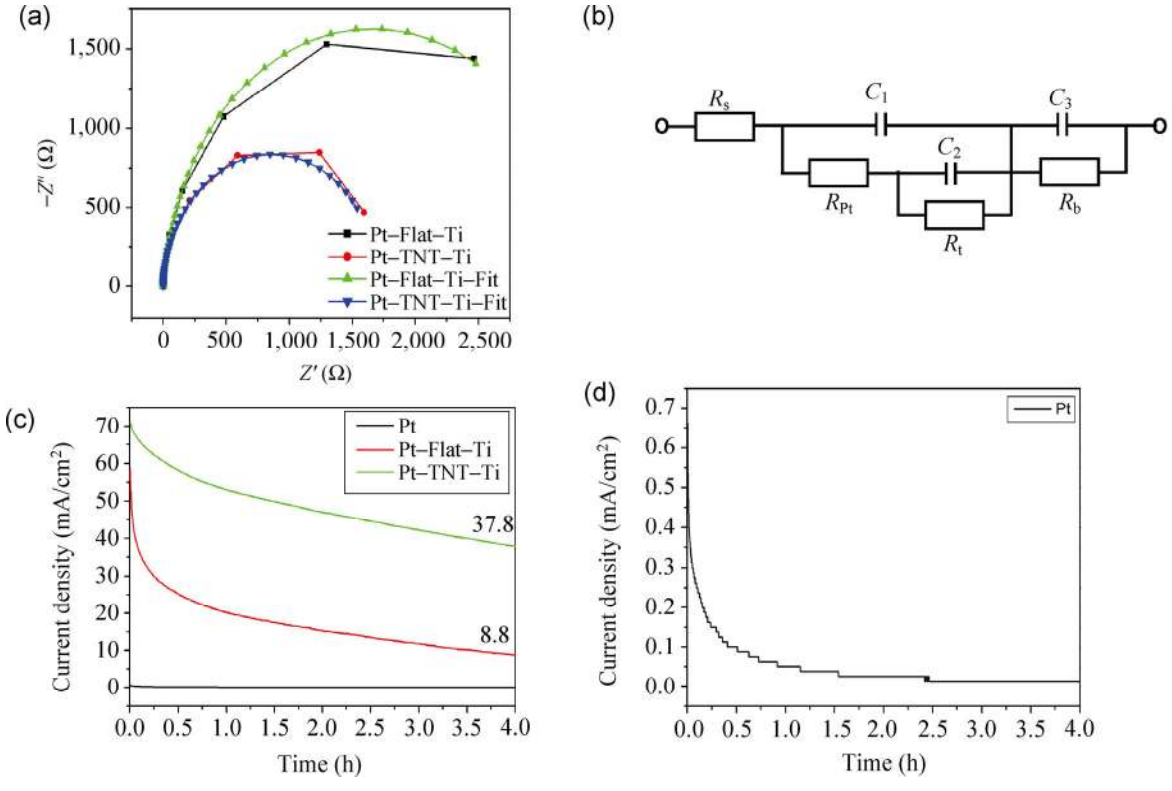

Figure 6 (a) EIS spectra for Pt–TNT–Ti and Pt–Flat–Ti tested in 1.0 M CH_3OH + 0.5 M H_2SO_4 solution. (b) Equivalent circuit for fitting values: R_s–solution resistance; R_{Pt}, C_1–for the surface Pt nanoflowers; R_t, C_2–for the TiO_2 nanotube layer or compact TiO_2 thin film; and R_b, C_3–for the titanium oxide barrier layer. (c) Chronoamperometric curves of Pt–TNT–Ti (green), Pt–Flat–Ti (red) and pure platinum (black) in 1.0 M CH_3OH + 0.5 M H_2SO_4 solution with a Pt loading 1.2176 mg/cm^2 for Pt–TNT–Ti and 0.9026 mg/cm^2 for Pt–Flat–Ti. (d) Chronoamperometric curve for pure platinum electrode.

Ti substrate of Pt–TNT–Ti is larger than that of Pt–Flat–Ti. This can be verified by the electrochemical impedance spectroscopy (EIS) results shown in Fig. 6(a), which were recorded at open circuit potential to get equilibrium information of these hybrid electrodes. The fitting parameters based on the equivalent circuit model in Fig. 6(b) are shown in Table 1. The resistance of the Pt (R_{Pt}) nanoflowers is 5.716 μΩ and 8.638 μΩ respectively for Pt–TNT–Ti and Pt–Flat–Ti. Also, the electron transport resistance (R_t) from the Pt nanoflowers to the TiO_2 nanotubes is 1.64 kΩ, lower than the electron transport resistance (3.25 kΩ) from the Pt nanoflowers to the TiO_2 flat film. These fitting parameters reproduce the smaller impedance semicircle of Pt–TNT–Ti compared to Pt–Flat–Ti. Zhang et al. [37] previously reported that Pt nanoflowers can be formed on conductive glass (indium tin oxide, ITO), and the reported electrode's anodic current density for oxidizing methanol is 14.7 mA/cm^2. Therefore, the electrocatalytic ability of our hybrid electrodes is about 10 times that of the previously reported results. The observed prominent anodic current can be partly attributed to the electrocatalytic activity of the Pt nanoflowers, which provide higher specific areas and more active centers for electrocatalysis. What is more, the Pt dispersed along the wall of the nanotubes improves the contact between Pt and the Ti substrate, resulting in improved conductivity of the hybrid electrode as confirmed by EIS.

The backward anodic current density peak (B_p) is 142.3 mA/cm^2 for Pt–TNT–Ti and 99.7 mA/cm^2 for Pt–Flat–Ti. The ratios (the higher value of this ratiois, the higher tolerance the electrode will have) of F_p to B_p are 1.051 for Pt–TNT–Ti and 0.963 for Pt–Flat–Ti electrodes, indicating slightly better carbon monoxide (CO) poisoning tolerance of Pt–TNT–Ti. It is widely recognized that pure Pt electrodes have an inherent tendency to suffer CO poisoning [38], which is also

Table 1 Fitting values of the equivalent circuit elements for Pt–TNT–Ti and Pt–Flat–Ti

Sample	R_s (mΩ)	R_b (Ω)	C_3 (mF)	R_t (kΩ)	C_2 (μF)	R_{Pt} (μΩ)	C_1 (mF)
Pt–TNT–Ti	304.5	61.26	26.45	1.64	448.2	5.716	2.765
Pt–Flat–Ti	445.5	38.04	15.71	3.25	393.4	8.638	2.427

R_s–solution resistance; R_{Pt}, C_1–for the surface Pt nanoflowers; R_t, C_2–for the TiO_2 nanotube layer for Pt–TNT–Ti or compact TiO_2 thin film for Pt–Flat–Ti; and R_b, C_3–for the compact titanium oxide barrier layer.

the case in our work (Fig. 5(b)). To overcome the CO poisoning problem, a Pt/Pd binary catalyst, one of the popular industrial electrodes [39, 40], was deposited on the surface of the TiO_2 nanotube thin film. The ratio of F_p to B_p, shown in Fig. S1 (in the ESM), was calculated to be 1.949 for Pt/Pd deposited on the TiO_2 nanotube thin film (Pt/Pd–TNT–Ti) and 1.497 for Pt/Pd deposited on the TiO_2 flat thin film (Pt/Pd–Flat–Ti). These ratios are higher than those for the pure Pt electrode on the same substrates, indicating that Pt/Pd binary nanoparticles can reduce CO poisoning problem.

Chronoamperometry data were recorded at 0.60 V vs. a standard calomel electrode (SCE) for 4 h as an investigation of the catalyst deactivation (Fig. 6(c)). The starting current density (S_{cd}) and the final current density (E_{cd}) of the samples are shown in Table S2 (in the ESM). Both Pt–TNT–Ti and Pt–Flat–Ti show a high initial current (70.867 mA/cm^2 for Pt–TNT–Ti and 58.404 mA/cm^2 for Pt–Flat–Ti). After reaction for 4 h however, the final currents decreased to 37.829 and 8.794 mA/cm^2 for Pt–TNT–Ti and Pt–Flat–Ti, respectively. The ratio of final current density to starting current density was calculated to be 0.534 and 0.151 respectively for Pt–TNT–Ti and Pt–Flat–Ti, compared to 0.018 for the Pt electrode. Both the Pt–TNT–Ti and Pt–Flat–Ti electrodes therefore exhibit slower current decay over time compared to the Pt electrode. This improvement can be attributed to a faster removal rate of the poisoning species on (110) facets of the Pt nanoflowers. In addition, Pt–TNT–Ti exhibits a slower current decay over time than Pt–Flat–Ti, revealing a higher chemomechanical stability. This is attributed to the slower rate of loss of Pt on Pt–TNT–Ti. Chronoamperometry data for Pt/Pd–TNT–Ti and Pt/Pd–Flat–Ti also revealed that the calculated ratios of final current density to starting current density were 0.636 and 0.373 respectively, indicating that TNT can improve the contact between the Pt/Pd catalysts and the Ti substrate.

The morphologies of Pt–TNT–Ti and Pt–Flat–Ti electrodes are shown in Fig. 7, which indicates that some Pt nanoflowers have been mechanically peeled off from Pt–Flat–Ti. This observation can be confirmed by the Pt loading, which was analyzed using inductively coupled plasma atomic-emission spectrometry (ICP) to be 1.2089 mg/cm^2 and 0.5058 mg/cm^2 for Pt–TNT–Ti and Pt–Flat–Ti respectively after the chronoamperometry observation. While Pt–Flat–Ti has lost 44% of its initial Pt, Pt–TNT–Ti loses only 0.7% of its initial Pt. The much higher loss rate of Pt loading for Pt–Flat–Ti (about 60 times that of Pt–TNT–Ti) is direct proof of the poorer mechanical contact between Pt nanoflowers and the flat TiO_2 surface. Both the morphology and the Pt loading for Pt–TNT–Ti are almost the same as in the as-deposited state, indicating a higher chemomechanical stability. A similar phenomenon was observed for Pt/Pd–TNT–Ti and Pt/Pd–Flat–Ti as well (Table S3 and Fig. S2 in the ESM).

The electrocatalytic activity of the samples after the chronoamperometry experiment was further measured by CV both in 0.5 M sulfuric acid solution and 1.0 M methanol plus 0.5 M sulfuric acid solution. Figure 4(c) gives the CV curves recorded in 0.5 M sulfuric acid solution. The CV behavior of Pt–TNT–Ti is almost identical to its as-deposited state, in contrast to a sharp decrease for Pt–Flat–Ti. The electrocatalytic active surface areas were calculated to be 214.913 cm^2/mg and 163.343 cm^2/mg for Pt–TNT–Ti and Pt–Flat–Ti, respectively. Figure 5(c) shows the CV curves tested in 1.0 M methanol plus 0.5 M sulfuric acid solution. The F_p for electro-oxidation of methanol decreased from 149.6 to 141.4 mA/cm^2 for Pt–TNT–Ti and from 96.0 to 54.9 mA/cm^2 for Pt–Flat–Ti electrodes. It was also found that the F_p peak current position for Pt–TNT–Ti shifted from 0.741 V to 0.764 V. This is attributed to CO poisoning which reduces the catalytic activity. The peak current position for Pt–Flat–Ti shifted from 0.717 V to 0.68 V, which is mainly attributed to Pt peeling off from the substrate. Peeling off of Pt decreases the oxidation current, resulting in decreasing

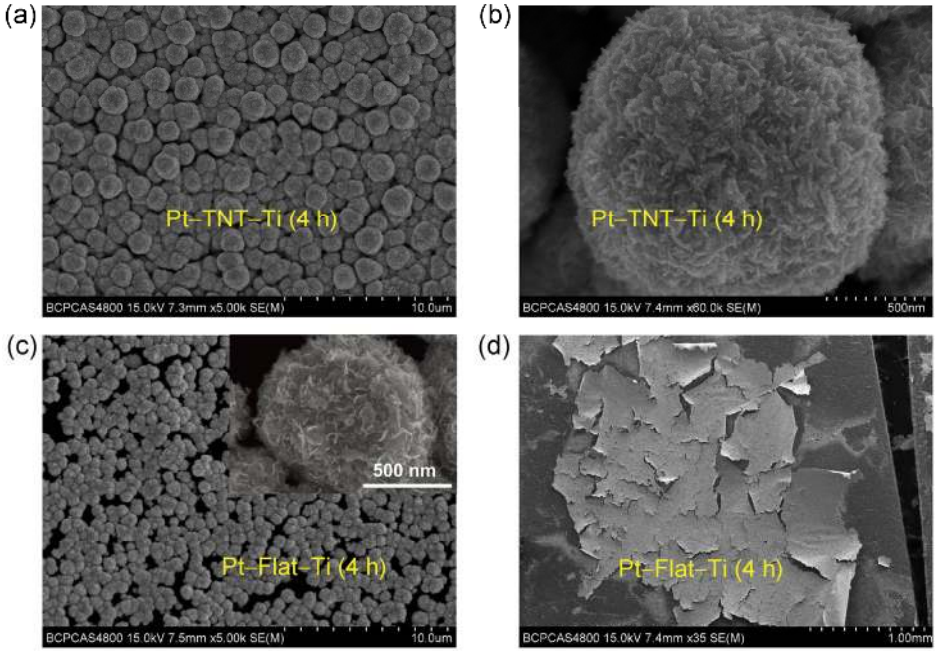

Figure 7 Morphologies of (a) and (b) Pt–TNT–Ti and (c) and (d) Pt–Flat–Ti after the chronoamperometric experiment.

resistance polarization, and exposes some new Pt surface, resulting in reduced CO poisoning. These observations verified that Pt–TNT–Ti exhibited higher mechanical stability than Pt–Flat–Ti. A similar phenomenon was found for Pt/Pd–TNT–Ti and Pt/Pd–Flat–Ti, as shown in Fig. S2 (in the ESM): F_p decreased from 304.4 to 283.9 mA/cm^2 for Pt/Pd–TNT–Ti and from 125.1 to 41.2 mA/cm^2 for Pt/Pd–Flat–Ti electrodes.

The above observations can be rationalized as follows. The cracks between Pt nanoflowers and flat TiO_2 passivation layer (Figs. 2(f) and 7(d)) result in the Pt nanoflowers being easily peeled off from the substrate. On the other hand, Pt nanoflowers were partly "planted" into TiO_2 nanotube arrays, resulting in more robust contact between Pt nanoflowers and the Ti substrate.

3 Conclusions

The surface of a Ti substrate has been nanostructured by forming TiO_2 nanotube arrays via anodizing. Pt nanoflowers were deposited on the nanostructured and non-nanostructured Ti substrates. Both the electrocatalytic activity and stability were greatly improved by nanostructuring the substrate surface, making the resulting materials attractive for electrochemical applications. What is more, the present work can provide a facile method to improve the quality of contact between other noble metals and metallic substrates.

4 Experimental details

4.1 Preparation of titanium dioxide nanotube (TNT) arrays

Ti foils (0.2 mm thickness, 99.7% purity, ordered from the General Research Institute for Nonferrous Metals (GRINM), China) were degreased by ultrasonic cleaning in acetone, ethanol and de-ionized (DI) water. The cleaned samples were dried in a nitrogen stream. Anodization was performed in an organic electrolyte of ethylene glycol containing 0.1 M NH_4HF_2 +0.5% DI water with a two-electrode cell. Ti foil was the working electrode, and a graphite foil served as a counter electrode. The voltage was 30 V and the duration was 4 h. The as-formed TiO_2 nanotube layers were annealed at 500 ℃ in air for 2 h with heating and cooling rates of 2 ℃/min [31, 32].

4.2 Preparation of Pt nanoflower structured electrodes

For Pt deposition, we used a current pulsing approach with a cathodic pulse (–350 mA, 6 ms), an anodic pulse (+350 mA, 1 ms) and a relaxation time (0 mA, 1 s) in 0.4 mM H_2PtCl_6 + 0.5 M H_2SO_4 aqueous electrolyte with a temperature of 30 ˚C for 10 min. The current pulse shape used in the present work is shown in Fig. 1(d). The electrolyte was strongly agitated with magnetic stirring during electrodeposition. The nano-flowered Pt was electrodeposited on the annealed TNT substrate (Pt–TNT–Ti). The Pt loading deposited was determined using inductively coupled plasma atomic-emission spectrometry (ICP-AES). The calculated Pt loading is 1.2176 mg/cm^2 for Pt–TNT–Ti (Table S4, in the ESM). For comparison, Pt nanoflowers were also electrodeposited on a Ti substrate with a flat TiO_2 thin film (Pt–Flat–Ti), which was formed via annealing titanium in an oxygen atmosphere at 500 ˚C for 2 h, and the Pt loading was measured as 0.9026 mg/cm^2. For comparison, the electrocatalytic capability of the pure platinum plate (Pt) with exposure area of 1 cm^2 was also investigated.

4.3 Structural characterization

The surface, top morphology and cross-section alignment of the samples were characterized using field emission scanning electron microscopy (Hitachi FE-SEM S4800) with an accelerating voltage of 15 kV. The phase compositions of the samples were determined by X-ray diffraction (XRD) using a diffractometer with copper (Cu) Kα radiation. The morphologies and microstructures of the samples were also observed by transmission electron microscopy (TEM) and high-resolution transmission electron microscopy (HRTEM, JEOL-2010, operated at 200 kV).

4.4 Electrochemical characterization

Active surface area was characterized by using an IM6EX Electrochemical Station (Zahner Instruments, Germany) in 0.5 M H_2SO_4 electrolyte. A traditional three-electrode system was used for the electrochemical tests, with the Pt–TNT–Ti hybrid electrode as the working electrode, a platinum plate (2 × 2 cm^2) as the counter electrode and a saturated calomel electrode (SCE) as the reference electrode. All potentials were reported against SCE.

The methanol electrocatalysis measurements were carried out using an IM6EX Electrochemical Station (Zahner Instruments, Germany) in 1.0 M CH_3OH plus 0.5 M H_2SO_4 electrolyte. A traditional three-electrode setup was used for the electrochemical tests, with the Pt–TNT–Ti hybrid electrode as the working electrode, a platinum plate (2 × 2 cm^2) as the counter electrode and a SCE as the reference electrode. All potentials were reported against SCE and all current densities were normalized to the electrode geometry area, or the nominal area of the electrode.

Electrochemical impedance spectroscopic (EIS) curves of the cells were measured in the frequency range from 0.1 Hz to 100 kHz under open circuit conditions. The test electrolyte was 1.0 M methanol plus 0.5 M sulfuric acid solution and the amplitude was 5 mV.

Acknowledgements

This work was financially supported by the National Outstanding Young Investigator Grant of China (No. 51225401), the National Natural Science Foundation of China (No. 51002004), the Beijing Municipal Commission of Education Foundation (Nos. KZ201010005001, KM201110005003). HYL also would like to acknowledge the fellowship from the China Scholarship Council and Rixin Talent authorized by Beijing University of Technology. JL acknowledges support by NSF DMR-1120901.

Electronic Supplementary Material: Supplementary material (methods, tables summarizing the Pt or Pt/Pd loading for different samples, active surface area and electrocatalytic oxidation for methanol in sulfuric acid solution) is available in the online version of this article at http://dx.doi.org/10.1007/s12274-014-0464-5.

References

[1] Steele, B. C. H.; Heinzel A. Materials for fuel cell technologies. *Nature* **2001**, *414*, 345–352.

[2] Wu, J. B.; Yang, H. Synthesis and electrocatalytic oxygen reduction properties of truncated octahedral Pt_3Ni nanoparticles. *Nano Res.* **2011**, *4*, 72–82.

[3] Wang, X. G.; Zhang, Z. H.; Tang, B.; Lin, N. M.; Hou, H. L.; Ma, Y. A facile preparation of novel Pt-decorated Ti electrode for methanol electro-oxidation by high-energy micro-arc cladding technique. *J. Power Sources* **2013**, *230*, 81–88.

[4] Tiwari, J. N.; Tiwari, R. N.; Lin, K. L. Controlled synthesis and growth of perfect platinum nanocubes using a pair of low-resistivity fastened silicon wafers and their electrocatalytic properties. *Nano Res.* **2011**, *4*, 541–549.

[5] Lu, Y. C.; Xu, Z. C.; Gasteiger, H. A.; Chen, S.; Kimberly, H. S.; Yang, S. H. Platinum–gold nanoparticles: A highly active bifunctional electrocatalyst for rechargeable lithium–air batteries. *J. Am. Chem. Soc.* **2010**, *132*, 12170–12171.

[6] Chen, Z.; Yu, A. P.; Higgins, D.; Li, H.; Wang, H. J.; Chen, Z. W. Highly active and durable core-corona structured bifunctional catalyst for rechargeable metal–air battery application. *Nano Lett.* **2012**, *12*, 1946–1952.

[7] Dong, S. M.; Chen, X.; Wang, S.; Gu, L.; Zhang, L. X.; Wang, X. G.; Zhou, X. H.; Liu, Z. H.; Han, P. X.; Duan, Y. L., et al. 1D coaxial platinum/titanium nitride nanotue arrays with enhanced electrocatalytic activity for the oxygen reduction reaction: Towards Li–air batteries. *ChemSusChem* **2012**, *5*, 1712–1715.

[8] Liu, H.; Xing, Y. C. Influence of Li ions on the oxygen reduction reaction of platinum electrocatalyst. *Electrochem. Commun.* **2011**, *13*, 646–649.

[9] Shirahata, S.; Hamasaki, T.; Teruya, K. Advanced research on the health benefit of reduced water. *Trends Food Sci. Tech.* **2012**, *23*, 124–131.

[10] Hamasaki, T.; Kashiwagi, T.; Imada, T.; Nakamichi, N.; Aramaki, S.; Toh, K.; Morisawa, S.; Shimakoshi, H.; Hisaeda, Y.; Shirahata, S. Kinetic analysis of superoxide anion radical-scavenging and hydroxyl radical-scavenging activities of platinum nanoparticles. *Langmuir* **2008**, *24*, 7354–7364.

[11] Hauch, A.; Georg, A. Diffusion in the electrolyte and charge-transfer reaction at the platinum electrode in dye-sensitized solar cells. *Electrochim. Acta* **2001**, *46*, 3457–3466.

[12] Fu, N. Q.; Fang, Y. Y.; Duan, Y. D.; Zhou, X. W.; Xiao, X. R.; Lin, Y. High-performance plastic platinized counter electrode via photoplatinization technique for flexible dye-sensitized solar cells. *ACS Nano* **2012**, *6*, 9596–9605.

[13] Zhang, S.; Ji, C. Y.; Bian, Z. Q.; Yu, P. R.; Zhang, L. H.; Liu, D. Y.; Shi, E. Z.; Shang, Y. Y.; Peng, H. T.; Cheng, Q. Porous, platinum nanoparticles-adsorbed carbon nanotube yarns for efficient fiber solar cells. *ACS Nano* **2012**, *6*, 7191–7198.

[14] Gong, Y.; Li, C. H.; Huang, X. M.; Luo, Y. H.; Li, D. M.; Meng, Q. B.; Iversen, B. B. Simple method for manufacturing Pt counter electrodes on conductive plastic substrates for dye-sensitized solar cells. *ACS Appl. Mater. Inter.* **2013**, *5*, 795–800.

[15] Hrapovic, S.; Liu, Y. L.; Male, K. B.; Luong, J. H. T. Electrochemical biosensing platforms using platinum nanoparticles and carbon nanotubes. *Anal. Chem.* **2004**, *76*, 1083–1088.

[16] Yang, M. H.; Yang, Y. H.; Liu, Y. L.; Shen, G. L.; Yu, R. Q. Platinum nanoparticles-doped sol–gel/carbon nanotubes composite electrochemical sensors and biosensors. *Biosens. Bioelectron.* **2006**, *21*, 1125–1131.

[17] Guo, S. J.; Wen, D.; Zhai, Y. M.; Dong, S. J.; Wang, E. K. Platinum nanoparticles ensemble-on-graphene hybrid nanosheet: One-pot, rapid synthesis, and used as new electrode materials for electrochemical sensing. *ACS Nano* **2010**, *4*, 3959–3968.

[18] Mondal, S.; Sangaranarayanan, M. V. A novel non-enzymatic sensor for urea using a polypyrrole-coated platinum electrode. *Sens. Actuators B* **2013**, *177*, 478–486.

[19] Kloke, A.; von Stetten, F.; Zengerle, R.; Kerzenmacher, S. Strategies for the fabrication of porous platinum electrode. *Adv. Mater.* **2011**, *23*, 4976–5008.

[20] Fu, G. T.; Wu, K.; Jiang, X.; Tao, L.; Chen, Y.; Lin, J.; Zhou, Y. M.; Wei, S. H.; Tang, Y. W.; Lu, T. H.; Xia, X. H. Polyallylamine-directed green synthesis of platinum nanocubes. Shape and electronic effect codependent enhanced electrocatalytic activity. *Phys. Chem. Chem. Phys.* **2013**, *15*, 3793–3802.

[21] Xu, J. F.; Fu, G. T.; Tang, Y. W.; Zhou, Y. M.; Chen, Y.; Lu, T. H. One-pot synthesis of three-dimensional platinum nanochain networks as stable and active electrocatalysts for oxygen reduction reactions. *J. Mater. Chem.* **2012**, *22*, 13585–13590.

[22] Gong, D. W.; Grimes, C. A.; Varghese, O. K.; Hu, W. C.; Singh, R. S.; Chen, Z.; Dickey, E. C. Titanium oxide nanotube arrays prepared by anodic oxidation. *J. Mater. Res.* **2001**, *16*, 3331–3334.

[23] Yang, M. J.; Zhu, J. L.; Liu, W.; Sun, J. L. Novel photodetectors based on double-walled carbon nanotube film/TiO_2 nanotube array heterodimensional contacts. *Nano Res.* **2011**, *4*, 901–907.

[24] Kim, J. Y.; Noh, J. H.; Zhu, K.; Halverson, A. F.; Neale, N. R.; Park, S.; Hong, K. S.; Frank A. J. General strategy for fabricating transparent TiO_2 nanotube arrays for dye-sensitized photoelectrodes: Illumination geometry and transport properties. *ACS Nano* **2011**, *5*, 2647–2656.

[25] Macak, J. M.; Tsuchiya, H.; Taveira, L.; Aldabergerova, S.; Schmuki, P. Smooth anodic TiO_2 nanotubes. *Angew. Chem. Int. Ed.* **2005**, *44*, 7463–7465.

[26] Guo, W. X.; Xue, X. Y.; Wang, S. H.; Lin, C. J.; Wang, Z. L. An integrated power pack of dye-sensitized solar cell and Li battery based on double-sided TiO_2 nanotube arrays. *Nano Lett.* **2012**, *12*, 2520–2523.

[27] Richter, C.; Schuttenmaer, C. A. Exciton-like trap states limit electron mobility in TiO_2 nanotubes. *Nat. Nanotechnol.* **2010**, *5*, 769–772.

[28] Li, H. Y.; Bai, X. D.; Ling, Y. H.; Li, J.; Zhang, D. L.; Wang, J. S. Fabrication of titania nanotubes as cathode protection for stainless steel. *Electrochem. Solid State Lett.* **2006**, *9*, B28–B31.

[29] Varghese, O. K.; Paulose, M.; Grimes, C. A. Long vertically aligned titania nanotubes on transparent conducting oxide for highly efficient solar cells. *Nat. Nanotechnol.* **2009**, *4*, 592–597.

[30] Lei, Y. Z.; Zhao, G. H.; Tong, X. L.; Liu, M. C.; Li, D. M.; Geng, R. High electrocatalytic activity of Pt–Pd binary spherocrystals chemically assembled in vertically alinghed TiO_2 nanotubes. *ChemPhysChem.* **2010**, *11*, 276–284.

[31] Li, H. Y.; Wang, J. S.; Huang, K. L.; Sun, G. S.; Zhou, M. L. In-situ preparation of multi-layer TiO_2 nanotube array thin films by anodic oxidation method. *Mater. Lett.* **2011**, *65*, 1188–1190.

[32] Wang, N.; Li, H. Y.; Lv, W. L.; Li, J. H.; Wang, J. S.; Zhang, Z. T.; Liu, Y. R. Effects of TiO_2 nanotubes with different diameters on gene expression and osseo-integration of implants in minipigs. *Biomaterials* **2011**, *32*, 6900–6911.

[33] Zhang, X. Y.; Dong, D. H.; Li, D.; Williams, T.; Wang, H. T.; Webley, P. A. Direct electrodeposition of Pt nanotube arrays and their enhanced electrocatalytic activities. *Electrochem. Commun.* **2009**, *11*, 190–193.

[34] Nielsch, K.; Muller, F.; Li, A. P.; Gosele, U. Uniform nickel deposition into ordered alumina pores by pulsed electrodeposition. *Adv. Mater.* **2000**, *12*, 582–586.

[35] Macak, J. M.; Gong, B. G.; Hueppe, M.; Schmuki, P. Filling of TiO_2 nanotubes by self-doping and electrodeposition. *Adv. Mater.* **2007**, *19*, 3027–3031.

[36] Song, Y. Y.; Gao, Z. D.; Schmuki, P. Highly uniform Pt nanoparticle decoration on TiO_2 nanotube arrays: A refresh-able platform for methanol electrooxidation. *Electrochem. Commun.* **2011**, *13*, 290–293.

[37] Zhang, H. M.; Zhou, W. Q.; Du, Y. K.; Yang, P.; Wang, C. Y. One-step electrodeposition of platinum nanoflowers and their high efficient catalytic activity for methanol electro-oxidation. *Electrochem. Commun.* **2010**, *12*, 882–885.

[38] Watanabe, M.; Motoo, S. Electrocatalysis by ad-atoms. 2. Enhancement of oxidation of methanol on platinum by ruthenium ad-atoms. *J. Electroanal. Chem.* **1975**, *60*, 267–273.

[39] Lim, B.; Jiang, M. J.; Carmargo, P. H. C.; Cho, E. C.; Tao, J.; Lu, X. M.; Zhu, Y. M.; Xia, Y. N. Pd–Pt bimetallic nanodendrites with high activity for oxygen reduction. *Science* **2009**, *324*, 1302–1305.

[40] Kim, G. B.; Jhi, S. H. Carbon monoxide-tolerant platinum nanoparticle catalysts on defect-engineered graphene. *ACS Nano* **2011**, *5*, 805–810.